Effects of omega-*O*-acylceramide structures and concentrations in healthy and diseased skin barrier lipid membrane models[S]

Lukáš Opálka,* Andrej Kováčik,* Petra Pullmannová,* Jaroslav Maixner,[†] and Kateřina Vávrová[1,*]

Charles University, Faculty of Pharmacy in Hradec Králové,* Hradec Králové, Czech Republic. University of Chemistry and Technology Prague,[†] Prague, Czech Republic

ORCID IDs: 0000-0003-1379-1406 (L.O.); 0000-0002-5597-3155 (A.K.); 0000-0001-5801-5094 (P.P.); 0000-0002-8502-4372 (K.V.)

Abstract **Ceramides (Cers) with ultralong (∼32-carbon) chains and ω-esterified linoleic acid, composing a subclass called omega-*O*-acylceramides (acylCers), are indispensable components of the skin barrier. Normal barriers typically contain acylCer concentrations of ∼10 mol%; diminished concentrations, along with altered or missing long periodicity lamellar phase (LPP), and increased permeability accompany an array of skin disorders, including atopic dermatitis, psoriasis, and ichthyoses. We developed model membranes to investigate the effects of the acylCer structure and concentration on skin lipid organization and permeability. The model membrane systems contained six to nine Cer subclasses as well as fatty acids, cholesterol, and cholesterol sulfate; acylCer content—namely, acylCers containing sphingosine (Cer EOS), dihydrosphingosine (Cer EOdS), and phytosphingosine (Cer EOP) ranged from zero to 30 mol%. Systems with normal physiologic concentrations of acylCer mixture mimicked the permeability and nanostructure of human skin lipids (with regard to LPP, chain order, and lateral packing). The models also showed that the sphingoid base in acylCer significantly affects the membrane architecture and permeability and that Cer EOP, notably, is a weaker barrier component than Cer EOS and Cer EOdS. Membranes with diminished or missing acylCers displayed some of the hallmarks of diseased skin lipid barriers (i.e., lack of LPP, less ordered lipids, less orthorhombic chain packing, and increased permeability). These results could inform the rational design of new and improved strategies for the barrier-targeted treatment of skin diseases.**—Opálka, L., A. Kováčik, P. Pullmannová, J. Maixner, and K. Vávrová. **Effects of omega-*O*-acylceramide structures and concentrations in healthy and diseased skin barrier lipid membrane models. *J. Lipid Res.* 2020.** 61: **219–228.**

Supplementary key words ceramides • epidermis • extracellular matrix • membranes/model • sphingolipids • acylceramide • disease models • permeability • membrane nanostructure

The uppermost human skin layer, the stratum corneum (SC), acts as a barrier against the penetration of potentially harmful substances, allergens, or bacteria into the organism and protects the body from excessive water loss (1). The major permeability barrier resides in the SC intercellular lipid matrix, which is an equimolar mixture of ceramides (Cers), FFAs, and cholesterol (Chol) with additional minor components, such as cholesteryl sulfate (CholS) (2–4). Cers represent a structurally heterogeneous group comprising at least 15 subclasses (supplemental Fig. S1). The most unusual members of the skin Cer family are the ω-*O*-acylceramides (acylCers or Cers of the EO subclass, **Fig. 1**). AcylCers have an ultralong ω-hydroxylated acyl chain (up to 38 carbons; usually 30–32 carbons) attached to a sphingoid base. Furthermore, linoleic acid is esterified to ω-hydroxyl (5), resulting in an acylCer total length of ∼70 carbons. AcylCers constitute ∼10 weight % (roughly 7 molar %) of the SC Cers (3, 6–8), although some studies report up to 25 weight % acylCer content (18 molar %) (9–12). The acylCers consist of sphingosine-based Cer EOS (∼51 weight %), phytosphingosine-based Cer EOP (∼11 weight %), dihydrosphingosine-based Cer EOdS (∼3 weight %) and 6-hydroxysphingosine-based Cer EOH (∼35 weight %) (3, 6–8).

This work was supported by the Czech Science Foundation (19-09135J) and the project Efficiency and safety improvement of current drugs and nutraceuticals: advanced methods – new challenge (EFSA-CDN) (CZ.02.1.01/0.0/0.0/16_019/0000841) co-funded by the European Regional Development Fund. The authors declare that they have no conflicts of interest with the contents of this article.

Manuscript received 23 September 2019 and in revised form 10 December 2019.

Published, JLR Papers in Press, December 19, 2019
DOI https://doi.org/10.1194/jlr.RA119000420

This article is available online at https://www.jlr.org

Abbreviations: acylCer, ω-*O*-acylceramide; Cer, ceramide; Cer EOdS, acylCers containing dihydrosphingosine; Cer EOP, acylCers containing phytosphingosine; Cer EOS, acylCers containing sphingosine; FTIR, Fourier transform infrared spectroscopy; Chol, cholesterol; CholS, sodium cholesteryl sulfate; IND, indomethacin; LPP long periodicity lamellar phase; SC, stratum corneum; SPP, short periodicity lamellar phase; TH, theophylline; XRD, X-ray diffraction.

[1] To whom correspondence should be addressed.
e-mail: katerina.vavrova@faf.cuni.cz.

[S] The online version of this article (available at https://www.jlr.org) contains a supplement.

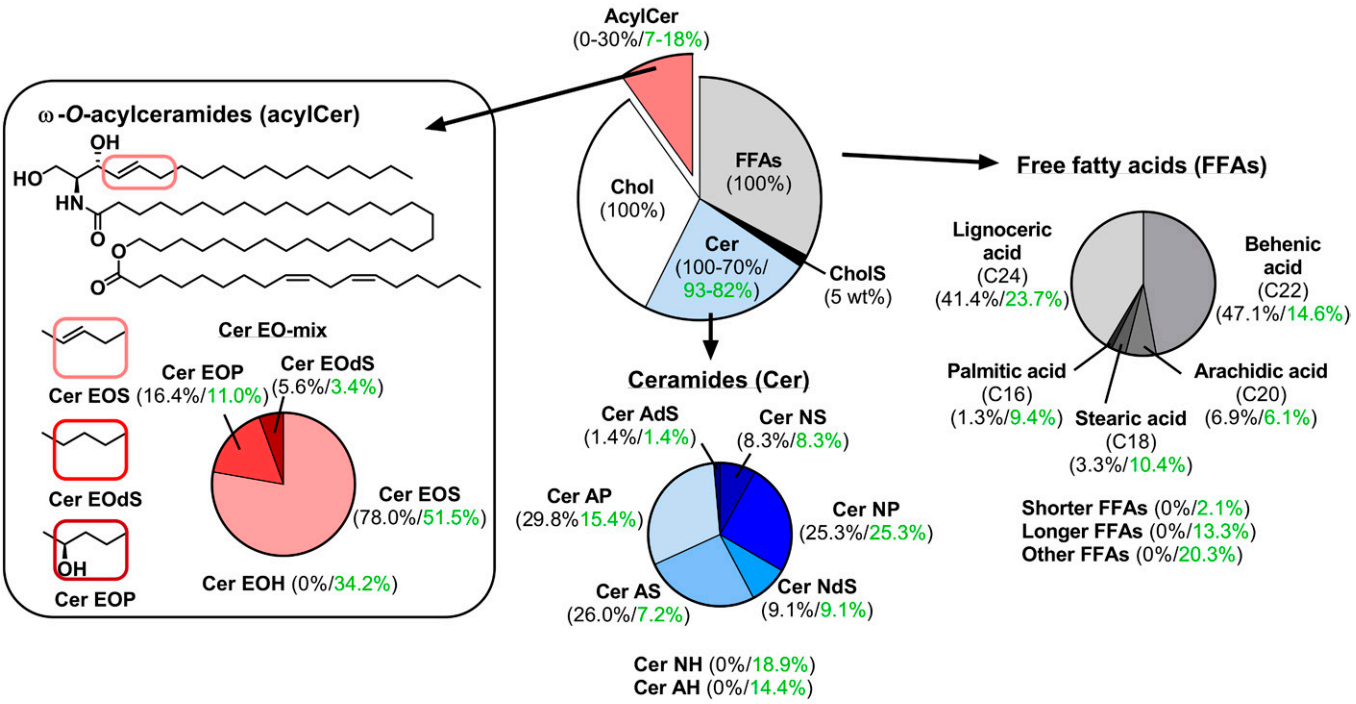

Fig. 1. Structures of the studied acylCers and the composition of the model lipid membranes (molar %). Green numbers indicate the composition of free human stratum corneum lipids (3, 6–8, 39).

AcylCers are indispensable for correct skin barrier functioning. A complete deficiency or major defects in the biosynthesis of acylCers lead to neonatal death due to enormous water loss through impaired skin (13, 14). Minor reductions in acylCer levels, accompanied by diminished long periodicity phase [LPP, a unique lamellar arrangement of skin lipids with 12–13 nm repeat distance (15–19)], and disturbed barrier function have been observed in several skin diseases (4) such as atopic dermatitis (20, 21), ichthyoses (22), psoriasis (23), Netherton syndrome (24), and dry skin (25). The acylCer levels in diseased and healthy skin vary among studies; the results depend on disease severity, sampling area, analytical method, and other factors. For example, acylCer levels were reduced by ∼50% (12, 26–28), ∼20% (10, 11), and 15% (21) in atopic dermatitis patients compared with healthy volunteers. Topical acylCers also have a strong potential in therapy for such diseases (29). Studies using isolated and synthetic ceramides showed that acylCers are crucial for the formation of LPP (16, 30–35) and acylCer headgroup architecture influences the LPP formation (31, 32). In our previous report, simple model membranes composed of Cer EOS/Cer NS/C_{24}-FFA/Chol/CholS closely reproduced the lamellar structure but not the permeability of the human skin barrier. Upon increasing the model complexity (6–9 Cer subclasses/FFAs/Chol/CholS), 10 molar % acylCers decreased the membrane permeability compared with that in the control without acylCers, as expected. Notably, only a mixture of acylCer EOS, EOdS and EOP, but not individual acylCers, formed both the LPP and orthorhombic chain packing at this concentration (30).

This study aims to shed light on the nontrivial relationships among the acylCer polar head structure, acylCer concentration, membrane nanostructure, and permeability. First, membrane models simulating healthy skin lipid barrier, containing 10–20 molar % acylCers (Cer EOS, EOP, EOds, or their mixture) of total Cer fraction were investigated. For information regarding the membrane composition, see Fig. 1. X-ray diffraction (XRD), Fourier transform infrared spectroscopy (FTIR), and the membrane permeabilities to water, two model permeants, and electrical impedance showed that these models reproduced the human skin lipid architecture (including LPP, lipid chain order, and lateral packing) and permeability. These healthy skin models were further compared with skin models with reduced acylCers (0 and 5 molar %), and models with an increased acylCer concentration (30 molar %).

MATERIALS AND METHODS

Chemicals

AcylCers [namely, Cer EOS (d18:1/h32:0/18:2), Cer EOP (t18:0/h32:0/18:2) and Cer EOdS (d18:0/h32:0/18:2)] (36) and Cer AdS (d18:0/h24:0) (37) were prepared according to published procedures. Cer NS (N-lignoceroyl-sphingosine; d18:1/24:0), Cer NP (N-lignoceroyl-phytosphingosine; t18:0/24:0), Cer AS (N-(2′-(R)-hydroxylignoceroyl)-sphingosine; d18:1/h24:0), Cer AP (N-(2′-(R)-hydroxylignoceroyl-phytosphingosine; t18:0/h24:0), and Cer NdS (N-lignoceroyl-dihydrosphingosine; d18:0/24:0) were purchased from Avanti Polar Lipids (Alabaster, AL). FFAs (lignoceric, docosanoic, eicosanoic, stearic, and palmitic acids), cholesterol, sodium cholesteryl sulfate, theophylline (TH), indomethacin

(IND), gentamycin sulfate, propylene glycol, buffer components, and solvents were purchased from Sigma-Aldrich (Schnelldorf, Germany). All solvents used were of analytical or high-performance LC (HPLC) grade. Water was purified using a Milli-Q system (Merck Millipore, Billerica, MA).

Preparation of model SC membranes

All membranes were prepared to mimic the lipid composition of human SC, i.e., an equimolar mixture of Cers/FFAs/Chol with 5 weight % CholS. The Cer fraction consisted of a very long chain Cer mixture (i.e., Cers NS, NP, AS, AP, NdS and AdS; Fig. 1) in the control sample, which was subsequently partially replaced with 5, 10, 20, or 30 molar % of acylCers (individual or mixture) in the test membranes. Due to the unavailability of Cers based on 6-hydroxysphingosine, these Cers were (proportionally) substituted with the available Cer subclasses as follows: Cer AS was used in place of Cer NH, and Cer AP was used in place of Cer AH (to maintain the same number of OH groups). AcylCer EOH was proportionally substituted with Cers EOS, EOdS, and EOP in the Cer EO-mix. FFAs of even chain lengths between 16 and 24C were mixed to simulate their SC proportions (Fig. 1) (38, 39).

The lipid solutions were mixed as shown in Fig. 1 and dried in a vacuum. Then, 1.35 mg of the lipid mixture was dissolved in 400 µl of hexane/96% ethanol 2:1 (v/v) and sprayed under a stream of nitrogen using a Linomat V (Camag, Muttenz, Switzerland) with additional y axis movement (38) on either a cover glass (22 × 22 mm) for XRD or Nuclepore polycarbonate filters (15 nm pore size, Whatman, Kent, Maidstone, UK) for the permeability experiments. The sprayed area was 1 cm^2, and the spraying flow rate was 10.2 µl/min. All prepared membranes were heated at 90°C, which is above their phase transition temperature, for 10 min and then slowly (overnight) cooled to 32°C. The membrane thickness was ~11 µm (40). Before the experiment, the membranes were equilibrated for at least 24 h at 32°C and 40–50% humidity (40, 41). The homogeneous lipid distribution between the center and the periphery of the lipid membrane was determined by high-performance TLC after the $CHCl_3$/MeOH (2:1 v/v) extraction of the specific part of the membrane (42).

XRD

The XRD of the studied lipid membranes was performed using an X'Pert PRO θ–θ powder diffractometer (PANanalytical B.V., Almelo, Netherlands) with parafocusing Bragg-Brentano geometry using CuK_α radiation (λ = 1.5418 Å, U = 40 kV, I = 30 mA) or CoK_α radiation (λ = 1.7903 Å, U = 35 kV, I = 40 mA). X-ray focus: type: line, length: 12 mm, width: 0.4 mm, take-off angle: 6°. Incident beam path: soller slit opening: 0.04 rad, beam mask width: 15 mm, automatic programmable divergence slit, irradiated length: 20 mm. Diffracted beam path: fixed anti-scatter slit height: 6.6 mm, soller slit opening: 0.04 rad, nickel filter thickness: 0.02 mm. Beam knife used at fixed height. The samples were mounted in modified sample holders (with inner diameter of 32 mm, for filters or solid samples with diameter of 30–32 mm, maximum thickness 5.8 mm) over the angular range of 0.6–30° (2 θ). The data were scanned with the ultrafast linear position-sensitive (1D) detector X'Celerator with a step size of 0.0167° (2 θ) and counting time of 20.32 s/step at room temperature. The data were evaluated using X'Pert Data Viewer (PANanalytical B.V., Almelo, The Netherlands). The XRD diffractograms show the scattered intensity as a function of the scattering vector Q [nm^{-1}], which is proportional to the scattering angle 2 θ according to the following equation: $Q = 4\pi \sin\theta/\lambda$ (λ = 0.15418 or 0.17903 nm is the wavelength of the X-rays). No correction factors were applied to the diffraction patterns. The repeat distance d [nm] characterizes the regular spacing of parallel lipid layers arranged on a one-dimensional lattice and was obtained from slope a of a linear regression fit of the dependence $Qn = a \times n + k$ according to the equation $d = 2\pi/a$. The peaks were assigned to a specific lamellar phase only when $R^2 \geq 0.9998$. This lipid arrangement is called a lamellar phase (L). The diffractograms of the lamellar phases exhibit a set of Bragg reflections whose reciprocal spacings are in the characteristic ratios of $Qn = 2\pi n/d$ (reflection's order number $n = 1, 2, 3\ldots$).

Transmembrane water loss, electrical impedance, and permeation experiments

Lipid membranes on support filters were fixed in Teflon® holders with a 0.5 cm^2 circular opening. The holders were mounted in Franz diffusion cells with the lipid layer facing the donor compartment. The acceptor parts of the cells at a 6.4 ± 0.1 ml volume (the precise volume was measured per cell and included in the calculations) were filled with PBS at pH = 7.4 with 50 mg/ml of gentamicin and equilibrated at 32°C for 12 h.

For the water loss measurement, the donor part of the cell was temporarily removed, and the TM 300 probe of the Cutometer MPA 580 (CK Electronic GmbH, Köln, Germany) was placed on top of the Teflon® membrane holder. The probe distance from the membrane was 0.6 cm, the effective measured area was 0.5 cm^2, the measurement time was set to 80 s (until the steady state was reached) and the value was recorded in grams per hour per meter squared. The measurements were carried out at 32 ± 0.5°C (temperature of the acceptor phase) in a box that excluded the air flow, at 26 ± 1°C ambient temperature and 40–50% air humidity.

Before the impedance measurement, 500 µl of PBS (pH = 7.4) were applied to the donor compartment on top of the lipid membrane, and the membranes were equilibrated at 32°C for 2 h. The impedance was measured using a 4080 LCR meter (Conrad Electronic, Hirschau, Germany) at an alternating frequency of 120 Hz and an error less than 0.5% (in the measuring range between 20 Ω and 10 MΩ). One stainless steel probe was placed in the acceptor compartment, the second probe was carefully placed in the buffer in the donor compartment, and the value was recorded in kΩ. The buffer from the donor compartment was carefully removed after the measurement using cotton swabs.

For the permeability experiments, 100 µl of a suspension of the model drug (either 5% TH or 2% IND in 60% propylene glycol) was applied on top of the lipid membrane in the donor compartment of the cell. The acceptor phase samples (300 µl) were collected every 2 h for 10 h and replaced with fresh PBS (this buffer replacement was included in the calculation of the flux). The typical lag times were below 2 h; thus, a 10 h experiment duration was sufficient to reach the steady state. The polycarbonate membrane had no effect on the permeability, and propylene glycol did not extract any lipids from the membrane, which was demonstrated using high-performance TLC (42).

HPLC

Samples containing TH and IND from the permeation experiments were analyzed using isocratic reverse-phase HPLC on a Shimadzu Prominence instrument (Shimadzu, Kyoto, Japan) with LC solution 1.22 software using a LiChroCART 250-4 column (LiChrospher 100 RP-18, 5 µm, Merck, Darmstadt, Germany) using validated methods (30, 41, 43). The separation of TH was achieved using 4:6 MeOH/0.1 M NaH_2PO_4 (v/v) at a flow rate of 1.2 ml/min. The column was maintained at 35°C. TH was detected at 272 nm; its retention time was 3.2 ± 0.1 min. For IND, 90:60:5 acetonitrile/water/acetic acid mobile phase was used at 2 ml/min, and the column was maintained at 40°C. IND was detected at 260 nm and its retention time was 3.1 ± 0.1 min.

FTIR

Selected lipid membranes were measured on a Nicolet 6700 spectrometer (Thermo Scientific) equipped with a single reflection

MIRacle ATR ZnSe crystal (PIKE Technologies, Madison, WI) and a clamping mechanism with constant pressure. The spectra were generated by the coaddition of 256 scans recorded at a 2 cm^{-1} resolution. Using a temperature control module (PIKE Technologies), the spectra were recorded between 28 and 100°C in 2°C steps (the stabilization time between steps was 6 min). The analysis was performed using Bruker OPUS software. The exact peak positions were determined from the second derivative spectra.

Data treatment

All data are presented as mean ± SEM. One-way ANOVA with Dunnett's post hoc test (indicated with * in the figures) or *t*-test (indicated with #) were used for the statistical analysis, and $P < 0.05$ was considered significant.

RESULTS

Long periodicity lamellar arrangement requires 30 molar % Cer EOP, 20 molar % Cer EOS/EOdS, but only 10 molar % of their mixture

First, the effects of individual acylCers and their mixture on the formation of the LPP arrangement were studied using XRD (**Fig. 2** and Supplemental Table S1). The control membrane comprised six very long Cer subclasses, five FFAs, Chol, and CholS (Fig. 1). In the test membranes, 5, 10, 20, or 30 molar % of the Cer fraction were replaced with the same molar proportion of acylCers; namely, Cer EOS, Cer EOP, Cer EOdS, or their mixture (EO-mix). The control membrane (0% acylCer) contained the following two series of reflections: short periodicity phase (SPP) with a repeat distance $d = 5.35–5.42$ nm and reflections at $Q = 1.86$ nm^{-1} and 3.69 nm^{-1} assigned to the separated Chol monohydrate ($d = 3.39–3.42$ nm) (44). The intensity distributions (peak shapes and amplitudes) depend on the XRD experimental setup (along with the sample properties) and cannot be directly compared with the intensity distributions reported in the literature.

The SPP repeat distance did not markedly change upon the acylCer incorporation in the membranes [$d = 5.33–5.42$ nm, which correlate with those found in SC lipid membranes, 5.4–5.5 nm (18, 31, 33)]. The Chol phase was also detected in all model membranes, which is consistent with the literature (25, 40, 45). Most samples also displayed another Chol peak at $Q = 6.74$ nm^{-1}, with Miller (hkl) indices [−111]. Some membranes (10–30 molar % Cer EO-mix, 5 molar % Cer EOS, 5 molar % Cer EOP, and 5, 10, 30 molar % Cer EOdS) showed a weak reflection at $Q = 1.33$ nm^{-1} (or a shoulder of the SPP first-order reflection; # in Fig. 2) corresponding to ∼4.7 nm. The precise identification of this peak was not possible due to the lack of other reflections; however, this phase represented a very minor component of the model membranes.

LPP formation strongly depended on the acylCer polar head structure (i.e., the sphingoid base) and concentration. In the membranes with the acylCer mixture (Cer EO-mix), LPP with $d = 12.31–12.88$ nm was found at 10 (in 3 of 4 samples), 20, and 30 molar % Cer EO-mix, along with SPP and Chol (Fig. 2A, E, and supplemental Table S1). In the model membranes with Cer EOS (Fig. 2B, F) and Cer EOdS (Fig. 2D, G), a 20 molar % acylCer concentration was required for LPP formation ($d = 12.31 – 12.85$ nm,

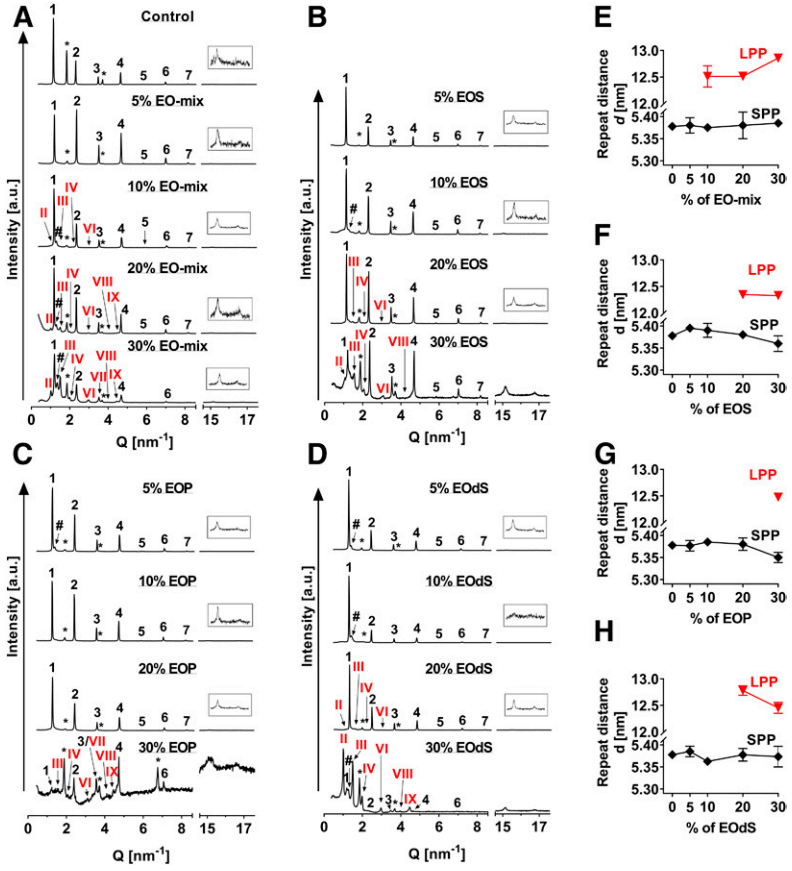

Fig. 2. Representative X-ray diffractograms, lamellar phases, and repeat distances found in the examined membranes with the acylCer mixture (EO-mix, A, E), Cer EOS (B, F), Cer EOP (C, G), and Cer EOdS (D, H). SPP, short periodicity phase (Arabic numerals), LPP, long periodicity phase (Roman numerals), Chol, phase of separated cholesterol (asterisks). # indicates an unidentified peak probably derived from separated behenic acid. Values are means ± SEM, n = 4.

supplemental Table S1). For Cer EOP, the LPP phase was only detectable in 2 of 4 samples at the highest studied concentration, i.e., 30 molar % Cer EOP, with d = 12.43–12.52 nm. Due to the technical limitations of the Bragg-Brentano geometry of our diffractometer, first- and second-order LPP reflections were usually not detected (46). However, we detected 4–7 higher order reflections enabling clear LPP assignment. We cannot exclude that, due to this limitation, some LPP that only gave the first- and second-order reflections was not detected, but this would apply only to a small fraction of lipids forming the LPP with a poor arrangement. All the LPP repeat distances were similar to those in murine SC (47), porcine SC (48), human SC (15, 49), and model membranes (16–19, 30, 33–35).

Wide-angle XRD (the region of the diffractogram between Q = 14 and 18 nm^{-1}) provides information about lipid chain packing (Fig. 2). Each membrane contained a reflection revealing the distance between planes of 0.412–0.415 nm, which originate from both orthorhombic and hexagonal packing. Membranes containing at least 10 molar % acylCers (or at least 20 molar % Cer EOP) also had a well-resolved reflection corresponding to the distance between planes of 0.373–0.375 nm, which (along with the former reflection) is indicative of an orthorhombic chain packing. The individual distances are shown in supplemental Table S2.

Additional hydroxyl in Cer EOP, compared with Cers EOS/EOdS, markedly changes the lipid chain order, packing, and membrane phase transitions

FTIR spectroscopy was used to probe the acylCer effects on the lipid chain order, packing, and phase transitions. All studied membranes had well-ordered lipid chains at 32°C (skin temperature) as suggested by the wavenumbers of the symmetric methylene stretching band below 2849 cm^{-1} (50) (**Fig. 3A**). Twenty molar % Cer EOS increased the lipid chain order compared with control (2848.5 cm^{-1}, which is by 0.3 cm^{-1} lower wavenumber than that of control; $P < 0.05$). A trend to improved lipid chain order (by 0.2 cm^{-1}; not significant) was also apparent in the membranes with Cer EOdS (Fig. 3A, B). In contrast, Cer EOP (at 20 and 30 molar %) rather disordered the lipid chains compared with Cer EOS at the same concentrations (by 0.3 cm^{-1}; $P = 0.05$). Such wavenumber shifts are rather small but relevant in the context of human skin lipids; for example, atopic dermatitis patients have by 0.4 cm^{-1} higher methylene symmetric stretching wavenumbers compared with healthy individuals (21).

The methylene stretching vibration is also sensitive to phase transitions, which are indicated by a marked increase in the band wavenumber. The control membrane without acylCers underwent a main order-to-disorder transition at 65°C (Fig. 3C). Upon the acylCer incorporation into the membranes, the transition temperatures did not significantly change (supplementary Fig. S2) and remained within the range of lipid transition temperatures (60–80°C) reported for intact human SC (51–53). Only with 30 molar % Cer EOP, the transition shifted to a higher temperature over the control (82°C, $P < 0.05$) and broadened, which is suggestive of noncooperative melting of different lipid domains

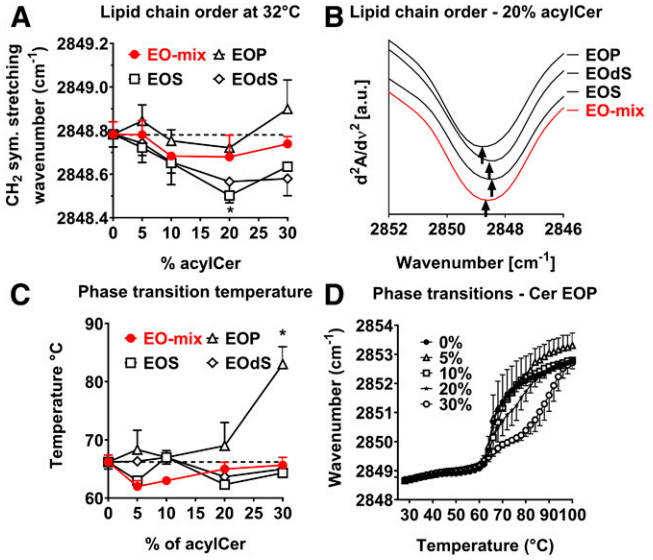

Fig. 3. FTIR spectroscopy of the lipid membranes showing the lipid chain order (A, B), phase transitions (C, D). A and B: methylene symmetric stretching wavenumbers at 32°C plotted against the acylCer concentration and example second derivative spectra of the methylene symmetric stretching of the membranes with 20 molar % acylCers, respectively (lower wavenumbers indicate more ordered lipids). C and D: order-to-disorder phase transition temperatures plotted against the acylCer concentration and methylene symmetric stretching wavenumbers of Cer EOP membranes plotted against temperature, respectively. The data are presented as means ± SEM, $n \geq 3$. Asterisks indicate statistically significant differences compared with the control at $P < 0.05$ (ANOVA).

(Fig. 3D). Similar but not significant behavior was observed with 20 molar % Cer EOP.

The methylene scissoring and rocking FTIR bands are sensitive to the lateral lipid arrangement (supplementary Figs. S3 and S4). In all studied membranes at 32°C with or without acylCers, the methylene scissoring band was split into a doublet (at ~1472 and 1465 cm^{-1}), which is due to the short-range vibrational coupling of the lipid chains packed in an orthorhombic subcell, and a central band at 1468 cm^{-1}, which is attributed to hexagonal lipid packing. This coexistence of orthorhombic and hexagonal packing is typical for SC lipids (54). Doublets indicative of orthorhombic packing were also observed in the methylene rocking bands (55) (at ~729 and 718 cm^{-1}). The band shapes indicate increased proportion of orthorhombic lipids with 10–20 molar % acylCers; for example, the scissoring doublet is ~1 cm^{-1} wider in 20% Cer EOS compared with control (50), but these changes could not be reliably quantified due to the complexity of the overlapping bands. Furthermore, the change in the proportion of orthorhombic lipids might also be due to a shift in the orthorhombic-hexagonal phase transition that takes place in the same temperature region.

Higher than physiological acylCer concentrations do not improve the barrier

The effects of acylCers on the membrane permeabilities were examined using four markers (**Fig. 4**, supplementary Table S3, and supplementary Fig. S5). TH is a representative small molecular exogenous permeant (MW = 180 g/mol)

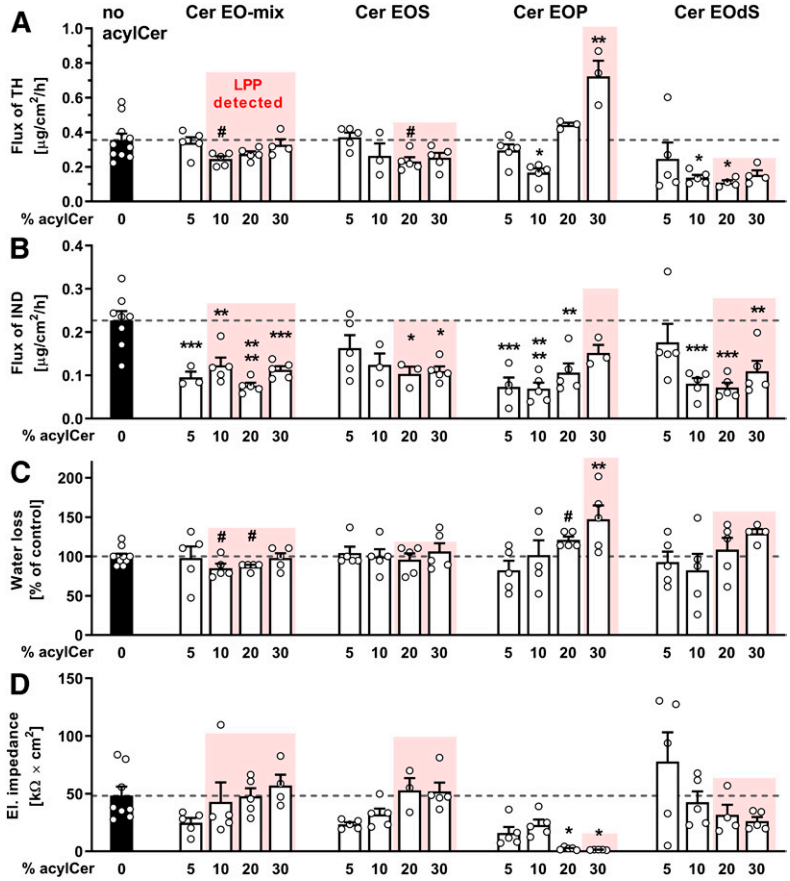

Fig. 4. Permeabilities of model lipid membranes containing Cer EO-mix, Cer EOS, Cer EOP, and Cer EOdS (at 5–30 molar % from the Cer fraction) compared with a control membrane without acylCers. A: Flux values of a model permeant TH. B: Flux values of a model permeant IND. C: Relative water loss through the membrane. D: Electrical impedance. Red shading of the bars indicates LPP presence. The data are presented as means ± SEM, n = 3–10. Asterisks indicate statistically significant differences compared with the control at *, $P < 0.05$; **, $P < 0.01$; ***, $P < 0.001$; and ****, $P < 0.0001$ (ANOVA). # indicates a statistically significant difference compared with the control at $P < 0.05$ (t-test).

with balanced hydrophilic and lipophilic behavior (log $P = -0.02$). The TH flux through the control membrane without acylCers was 0.36 μg/cm^2/h (Fig. 4A, supplementary Table S3). With the Cer EO-mix in the membranes, the flux decreased at 10 molar %, and then slowly increased, reaching values similar to those in the control at 30 molar % Cer EO-mix. With Cer EOS in the membranes, TH flux reached minimum at 20 molar % Cer EOS. Cer EOdS, which lacks a double bond compared with Cer EOS, led to the lowest permeabilities to TH among all studied membranes (with minimum at a 20 molar % concentration). With Cer EOP (which has an additional hydroxyl at C4 compared with Cer EOdS), the permeabilities to TH decreased at 10 molar % Cer EOP but then markedly increased, reaching 0.72 μg/cm^2/h at 30 molar % Cer EOP.

IND is a relatively large lipophilic molecule (MW = 358 g/mol, log P = 3.8). The IND flux through the control membrane was 0.23 μg/cm^2/h (Fig. 4B, supplementary Table S3). The Cer EO-mix significantly reduced the IND flux; the membrane with 20 molar % Cer EO-mix had an almost three-times stronger barrier than the control. In the Cer EOS and Cer EOdS membranes, the minima were also reached at 20 molar %. Cer EOP initially decreased the IND flux at 5–10 molar % concentration and then increased it at 30 molar % Cer EOP.

Water loss through the control membrane was set to 100% (Fig. 4C). In the membranes with 10–20 molar % Cer EO-mix, the water loss decreased by 12–13%. Cer EOS or Cer EOdS did not significantly change the water loss at any concentration studied, whereas 30 molar % Cer EOP increased the water permeability by almost 50%. The electrical impedance did not reveal significant differences among the membranes, except for 20 and 30 molar % Cer EOP, which decreased the values by an order of magnitude compared with that in the control (Fig. 4D).

DISCUSSION

Models with 10–20 molar % acylCers mimic the nanostructure and permeability of healthy skin barrier lipids

The characteristic composition and organization of intercellular SC lipids are essential for the barrier function of human skin. AcylCers, which constitute an epidermal-specific subclass of Cers with ultralong ω-hydroxylated chains esterified with linoleic acid, represent an indispensable component of the skin lipid barrier. Despite numerous reports of diminished acylCers in skin diseases, due to the complexity of lipid alterations in such diseases, elucidating the relationships among the acylCer polar head structure, acylCer concentration, SC lipid organization, and permeability is challenging.

Here, we studied model membranes with 6–9 Cer subclasses, including acylCers (namely, Cer EOS, EOdS, EOP, and their close-to-physiological mixture, Cer EO-mix; each at 0–30 molar % of the Cer mixture), FFAs, Chol, and CholS. The acylCer mixture induced LPP formation at 10 molar %, Cer EOS and EOdS at 20 molar %, whereas the phytosphingosine-based Cer EOP only promoted this lamellar phase at 30 molar % of the Cer fraction. This

behavior indicates the advantage of a polar head heterogeneity in acylCers in the skin barrier, and a lessened ability of Cer EOP to form LPP compared with Cer EOS. The lack of LPP in the system with 10 molar % Cer EOS contrasts previous studies using membranes composed of Cer EOS/Cer NP/bovine brain Cer/FFA mixture/Chol (31) or Cer EOS/Cer NS/lignoceric acid/Chol/CholS (30), where the LPP was formed at 5 and 10 molar % concentration, respectively. Thus, both membrane composition and preparation procedure appear to play important roles in whether LPP is formed; this behavior is currently under investigation.

Human SC lipid chains are well ordered (typical infrared methylene symmetric stretching values around 2849 cm^{-1}) (21) and tightly organized in orthorhombic packing (56, 57). The models with close-to-physiological concentrations of Cer EO-mix (and also with Cer EOS and Cer EOdS) reproduced both the SC lipid chain order and packing. The lipid packing in the model with Cer EOP appeared less tight and the phase transition in the model with 20% Cer EOP suggested a formation of separated domains.

The permeabilities of the models with 10–20 molar % Cer EO-mix were in good agreement with the membranes with isolated Cers from human SC (flux values of TH and IND were 0.25 ± 0.03 $\mu g/cm^2/h$ and 0.09 ± 0.01 $\mu g/cm^2/h$, respectively) (58). Thus, the lipid systems with 10–20 molar % Cer EO-mix reproduced the lamellar phases, chain order, lateral packing, and permeability of human skin lipids. In the membrane with 20 molar % Cer EOP, a weaker barrier compared with the membranes with Cer EOS and Cer EOdS was found, which is consistent with the lack of LPP and less tight packing in the EOP sample. Notably, LPP formation in the membranes with 10 molar % Cer EO-mix and 20 molar % Cers EOS/EOdS coincided with the minima in their permeabilities. However, considering the permeabilities of the membranes with Cer EOS and Cer EOdS at 10 molar % (i.e., without LPP) and 20 molar % (with LPP), we cannot conclude that LPP formation per se decreases membrane permeability (at least not to the markers investigated here). To better understand this behavior, we prepared membranes with either decreased or increased acylCer content.

Models with 0–5 molar % acylCers mimic some hallmarks of diseased skin lipid barrier (lack of LPP, less ordered lipids, less tight lipid packing and increased permeability)

The reduction in the acylCer content has been found in numerous skin diseases (4, 59), for example in atopic dermatitis (6, 10, 11, 20, 21, 60). In this inflammatory skin disease, LPP was diminished or absent, lipids were less ordered (by 0.4 cm^{-1} higher methylene symmetric stretching wavenumber) and less tightly packed (reduced width of the methylene scissoring vibration by 1 cm^{-1}) compared with healthy individuals (21). These structural changes were accompanied by increased transepidermal water loss [by up to 33% (11), by 10% (61), or 2- to 3-fold compared with healthy skin (6, 20, 21)] and 2- to 3.5-fold higher permeation of various compounds [e.g., TH (62), sodium lauryl sulfate, polyethylene glycols, various dyes; reviewed in Ref. (63)]. Thus, we prepared lipid models with reduced acylCer content (to 0–5 molar %) to see whether such models reasonably reproduce the above-mentioned disease features (disturbed lipid organization and increased permeability compared with models with 10–20% acylCers). One cannot expect a lipid model to provide results quantitatively comparable to data found in diseased skin as the model membranes do not contain corneocytes or corneocyte lipid envelopes, and more lipid abnormalities influence permeability in atopic skin in addition to reduced acylCers [e.g., Cers and FFAs with shortened chains (21), unsaturated FFAs (64) or changes in the covalent lipid envelope (10)]. In addition, the missing acylCers in the model were replaced by the Cer mixture. Therefore, the changes described here can be solely attributed to the lack of particular acylCer molecules and not to fewer lipids or disturbed Cers/FFAs/Chol ratios.

The membrane without acylCers arranged into SPP and Chol phase, which is consistent with previous findings (30, 41, 65) as LPP requires acylCers (30, 32, 66). Previously, a small fraction of lipids formed the LPP upon the incorporation of 5 molar % Cer EOS in model membranes composed of an equimolar mixture of Cers (EOS, NP, and bovine brain Cer in a 1:7:2 ratio), FFA mixture, and Chol (31). However, in our membrane model, the substitution of 5 molar % of the Cer mixture with acylCers either with a single acylCer (EOS, EOP, or EOdS) or a mixture (Cer EO-mix) was not sufficient to form LPP. This discrepancy may be due to differences in lipid composition and sample preparation. In addition, the small shift in the methylene symmetric stretching wavenumber (by up to 0.4 cm^{-1}) indicates a slightly decreased lipid chain order associated with reduced acylCers compared with that in membranes with close-to-physiologic acylCer concentrations.

The permeabilities of our membranes with 0–5 molar % Cer EO-mix to TH, IND, and water were ~40% higher, ~100, and by 30% higher, respectively, than those with 10 molar % Cer EO-mix, which is the composition closest to that of the native skin lipid barrier. Thus, the lipid systems with 0–5 molar % acylCers reasonably reproduced both the altered lipid nanostructure (lack of LPP, less ordered lipids, and less orthorhombic chain packing) and increased permeability, which are some of the hallmarks of skin diseases associated with reduced acylCer content. These results also suggest that TH and IND are apparently complementary markers that respond differently to changes in the membrane composition probably because of their different permeation pathways (67) and because acylCers strongly reinforce the inward permeability barrier to lipophilic compounds.

Increased acylCer content (30 molar %) does not improve the barrier but reveals structure-activity relationships among acylCers

Furthermore, we were interested in determining whether increased concentrations of acylCers could further promote LPP formation and reinforce the barrier. We prepared membranes with 30 molar % acylCers, as such high acylCer concentrations (or even higher) have been used in experiments investigating the LPP structure (18, 19, 68, 69).

At 30 molar % acylCers, either single or mixed, LPP, SPP, and the Chol phase were observed in all studied membranes. Similar results were observed by Neto et al. (18) in model membranes composed of an equimolar mixture of Cers (containing 30 molar % Cer EOS), FFA mixture, and Chol, and they reported LPP as the dominant phase, accompanied by a minor fraction of a separated Chol phase and one reflection of SPP. The persistence of SPP in all our model membranes at 30 molar % of acylCers contrasts with previous studies using membranes with simpler composition [Cer EOS, Cer NS, lignoceric acid, Chol and CholS (30)] or higher proportion of Cer EOS (40 molar %) (19). The differences between these studies may be caused by the variations in the lipid composition and membrane preparation. Notably, the XRD peak intensities in the membranes with 30% acylCers were rather low, indicating that the fraction of regularly organized lipids was diminished. This behavior is supported by the apparent trends in FTIR to diminished chain order and packing at 30% acylCers and permeability data. This effect of 30% acylCers may be connected with the limited heterogeneity in the lipid chain lengths or membrane preparation method.

Despite the LPP presence in all studied membranes at the 30 molar % acylCer content, their permeabilities were strongly affected by the acylCer polar head structure. The membranes with 30 molar % Cer EO-mix, Cer EOS, and Cer EOdS had similar permeabilities to the membranes with close-to-physiological acylCer concentrations. In contrast, a rather weak barrier (to TH, water, and electrical current) was found in the membrane with 30 molar % Cer EOP. Thus, the LPP formed at 30 molar % Cer EOP is either organized differently than the LPP induced by Cer EOS, Cer EOdS, or Cer EO-mix (although they have similar repeat distances) or is accompanied by structural alterations not detectable by XRD. In fact, 30 molar % Cer EOP likely induced phase separation. As the additional separated phase was not observed by XRD, it probably lacked a periodically repeating structure, which may explain the negative effects of Cer EOP on the membrane permeability.

Apparently, C4-C5 unsaturation in Cer EOS does not have significant influence on the lipid arrangement into LPP, whereas C4 hydroxyl disturbs the ability of Cer EOP to organize in this manner. This Cer EOP behavior is correlated with previous finding that Cer EOP has decreased ability to form LPP compared with Cer EOS and that Cer EOP can, at least partly, phase separate (31). Pure Cer EOP also forms a stronger hydrogen bond network than Cer EOS and more readily organizes into an LPP-like phase with 12.5 nm periodicity without other skin barrier lipids (17). The different relative contributions of hydrogen bonding and chain packing in the organization of phytosphingosine Cer and sphingosine Cer have been discussed previously (70, 71). Thus, the LPP observed in our 30 molar % Cer EOP membranes might actually be a separated Cer EOP-rich phase. Cer EOP appears to be the weakest barrier component among the acylCers studied here. This unfavorable behavior of Cer EOP likely explains why skin prefers to synthesize Cer EOS (∼50% acylCers) over Cer EOP (∼10%) although the amounts of other phytosphingosine Cers such as Cer NP and Cer AP in the skin barrier are rather high.

We thank Mrs. Iva Vencovská for technical assistance.

REFERENCES

1. Madison, K. C. 2003. Barrier function of the skin: "la raison d'etre" of the epidermis. *J. Invest. Dermatol.* **121:** 231–241.
2. Elias, P. M. 1991. Epidermal barrier function: intercellular lamellar lipid structures, origin, composition and metabolism. *J. Control. Release.* **15:** 199–208.
3. Masukawa, Y., H. Narita, H. Sato, A. Naoe, N. Kondo, Y. Sugai, T. Oba, R. Homma, J. Ishikawa, Y. Takagi, and T. Kitahara. 2009. Comprehensive quantification of ceramide species in human stratum corneum. *J. Lipid Res.* **50:** 1708–1719.
4. van Smeden J., M. Janssens, G. S. Gooris, and J. A. Bouwstra. 2014. The important role of stratum corneum lipids for the cutaneous barrier function. *Biochim. Biophys. Acta Mol. Cell. Biol.* **1841:** 295–313.
5. van Smeden J, W. A. Boiten, T. Hankemeier, R. Rissmann, J. A. Bouwstra, and R. J. Vreeken. 2014. Combined LC/MS-platform for analysis of all major stratum corneum lipids, and the profiling of skin substitutes. *Biochim. Biophys. Acta Mol. Cell. Biol.* **1841:** 70–79.
6. Ishikawa, J., H. Narita, N. Kondo, M. Hotta, Y. Takagi, Y. Masukawa, T. Kitahara, Y. Takema, S. Koyano, S. Yamazaki, and A. Hatamochi. 2010. Changes in the ceramide profile of atopic dermatitis patients. *J. Invest. Dermatol.* **130:** 2511–2514.
7. Janssens, M., J. van Smeden, G. S. Gooris, W. Bras, G. Portale, P. J. Caspers, R. J. Vreeken, S. Kezic, A. P. Lavrijsen, and J. A. Bouwstra. 2011. Lamellar lipid organization and ceramide composition in the stratum corneum of patients with atopic eczema. *J. Invest. Dermatol.* **131:** 2136–2138.
8. t'Kindt R., L. Jorge, E. Dumont, P. Couturon, F. David, P. Sandra, and K. Sandra. 2012. Profiling and characterizing skin ceramides using reversed-phase liquid chromatography-quadrupole time-of-flight mass spectrometry. *Anal. Chem.* **84:** 403–411.
9. Farwanah, H., K. Raith, R. H. Neubert, and J. Wohlrab. 2005. Ceramide profiles of the uninvolved skin in atopic dermatitis and psoriasis are comparable to those of healthy skin. *Arch. Dermatol. Res.* **296:** 514–521.
10. Macheleidt, O., H. W. Kaiser, and K. Sandhoff. 2002. Deficiency of epidermal protein-bound omega-hydroxyceramides in atopic dermatitis. *J. Invest. Dermatol.* **119:** 166–173.
11. Jungersted, J., H. Scheer, M. Mempel, H. Baurecht, L. Cifuentes, J. Høgh, L. I. Hellgren, G. B. Jemec, T. Agner, and S. Weidinger. 2010. Stratum corneum lipids, skin barrier function and filaggrin mutations in patients with atopic eczema. *Allergy.* **65:** 911–918.
12. Yamamoto, A., S. Serizawa, M. Ito, and Y. Sato. 1991. Stratum corneum lipid abnormalities in atopic dermatitis. *Arch. Dermatol. Res.* **283:** 219–223.
13. Jennemann, R., M. Rabionet, K. Gorgas, S. Epstein, A. Dalpke, U. Rothermel, A. Bayerle, F. van der Hoeven, S. Imgrund, J. Kirsch, et al. 2012. Loss of ceramide synthase 3 causes lethal skin barrier disruption. *Hum. Mol. Genet.* **21:** 586–608.
14. Vasireddy, V., Y. Uchida, N. Salem, S. Y. Kim, M. N. A. Mandal, G. B. Reddy, R. Bodepudi, N. L. Alderson, J.C. Brown, H. Hama, et al. 2007. Loss of functional ELOVL4 depletes very long-chain fatty acids (≥ C28) and the unique ω-O-acylceramides in skin leading to neonatal death. *Hum. Mol. Genet.* **16:** 471–482.
15. Bouwstra, J. A., G. S. Gooris, J. A. Vanderspek, and W. Bras. 1991. Structural investigations of human stratum-corneum by small-angle X-ray-scattering. *J. Invest. Dermatol.* **97:** 1005–1012.
16. McIntosh, T. J., M. E. Stewart, and D. T. Downing. 1996. X-ray diffraction analysis of isolated skin lipids: Reconstitution of intercellular lipid domains. *Biochemistry.* **35:** 3649–3653.
17. Kessner, D., G. Brezesinski, S. S. Funari, B. Dobner, and R. H. Neubert. 2010. Impact of the long chain ω-acylceramides on the stratum corneum lipid nanostructure. Part 1: Thermotropic phase behaviour of CER [EOS] and CER [EOP] studied using X-ray powder diffraction and FT-Raman spectroscopy. *Chem. Phys. Lipids.* **163:** 42–50.
18. de Sousa Neto, D., G. Gooris, and J. Bouwstra. 2011. Effect of the omega-acylceramides on the lipid organization of stratum corneum

model membranes evaluated by X-ray diffraction and FTIR studies (Part I). *Chem. Phys. Lipids.* **164:** 184–195.
19. Mojumdar, E. H., G. S. Gooris, D. J. Barlow, M. J. Lawrence, B. Deme, and J. A. Bouwstra. 2015. Skin lipids: localization of ceramide and fatty acid in the unit cell of the long periodicity phase. *Biophys. J.* **108:** 2670–2679.
20. Di Nardo, A., P. Wertz, A. Giannetti, and S. Seidenari. 1998. Ceramide and cholesterol composition of the skin of patients with atopic dermatitis. *Acta Derm. Venereol.* **78:** 27–30.
21. Janssens, M., J. van Smeden, G. S. Gooris, W. Bras, G. Portale, P. J. Caspers, R. J. Vreeken, T. Hankemeier, S. Kezic, R. Wolterbeek, et al. 2012. Increase in short-chain ceramides correlates with an altered lipid organization and decreased barrier function in atopic eczema patients. *J. Lipid Res.* **53:** 2755–2766.
22. Paige, D., N. Morse-Fisher, and J. Harper. 1994. Quantification of stratum corneum ceramides and lipid envelope ceramides in the hereditary ichthyoses. *Br. J. Dermatol.* **131:** 23–27.
23. Motta, S., M. Monti, S. Sesana, R. Caputo, S. Carelli, and R. Ghidoni. 1993. Ceramide composition of the psoriatic scale. *Biochim. Biophys. Acta.* **1182:** 147–151.
24. van Smeden, J., M. Janssens, W. A. Boiten, V. van Drongelen, L. Furio, R. J. Vreeken, A. Hovnanian, and J. A. Bouwstra. 2014. Intercellular skin barrier lipid composition and organization in Netherton syndrome patients. *J. Invest. Dermatol.* **134:** 1238–1245.
25. Schreiner, V., G. S. Gooris, S. Pfeiffer, G. Lanzendörfer, H. Wenck, W. Diembeck, E. Proksch, and J. Bouwstra. 2000. Barrier characteristics of different human skin types investigated with X-ray diffraction, lipid analysis, and electron microscopy imaging. *J. Invest. Dermatol.* **114:** 654–660.
26. Matsumoto, M., N. Umemoto, H. Sugiura, and M. Uehara. 1999. Difference in ceramide composition between "dry" and "normal" skin in patients with atopic dermatitis. *Acta Derm. Venereol.* **79:** 246–247.
27. Bleck, O., D. Abeck, J. Ring, U. Hoppe, J-P. Vietzke, R. Wolber, O. Brandt, and V. Schreiner. 1999. Two ceramide subfractions detectable in Cer (AS) position by HPTLC in skin surface lipids of nonlesional skin of atopic eczema. *J. Invest. Dermatol.* **113:** 894–900.
28. Imokawa, G., A. Abe, K. Jin, Y. Higaki, M. Kawashima, and A. Hidano. 1991. Decreased level of ceramides in stratum corneum of atopic dermatitis: an etiologic factor in atopic dry skin? *J. Invest. Dermatol.* **96:** 523–526.
29. Mauldin, E. A., D. Crumrine, M. L. Casal, S. Jeong, L. Opálka, K. Vavrova, Y. Uchida, K. Park, B. Craiglow, K. A. Choate et al. 2018. Cellular and metabolic basis for the ichthyotic phenotype in NIPAL4 (ichthyin)-deficient canines. *Am. J. Pathol.* **188:** 1419–1429.
30. Opálka, L., A. Kováčik, J. Maixner, and K. Vávrová. 2016. Omega-O-acylceramides in skin lipid membranes: effects of concentration, sphingoid base, and model complexity on microstructure and permeability. *Langmuir.* **32:** 12894–12904.
31. de Jager, M., G. Gooris, M. Ponec, and J. Bouwstra. 2004. Acylceramide head group architecture affects lipid organization in synthetic ceramide mixtures. *J. Invest. Dermatol.* **123:** 911–916.
32. de Jager, M. W., G. S. Gooris, M. Ponec, and J. A. Bouwstra. 2005. Lipid mixtures prepared with well-defined synthetic ceramides closely mimic the unique stratum corneum lipid phase behavior. *J. Lipid Res.* **46:** 2649–2656.
33. Bouwstra, J. A., G. S. Gooris, F. E. R. Dubbelaar, A. M. Weerheim, A. P. Ijzerman, and M. Ponec. 1998. Role of ceramide 1 in the molecular organization of the stratum corneum lipids. *J. Lipid Res.* **39:** 186–196.
34. Bouwstra, J. A., G. S. Gooris, K. Cheng, A. Weerheim, W. Bras, and M. Ponec. 1996. Phase behavior of isolated skin lipids. *J. Lipid Res.* **37:** 999–1011.
35. Bouwstra, J. A., K. Cheng, G. Gooris, A. Weerheim, and M. Ponec. 1996. The role of ceramides 1 and 2 in the stratum corneum lipid organisation. Biochim. Biophys. Acta. **1300:** 177–186.
36. Opálka, L., A. Kováčik, M. Sochorová, J. Roh, J. Kuneš, J. Lenčo, and K. Vávrová. 2015. Scalable Synthesis of Human Ultralong Chain Ceramides. *Org. Lett.* **17:** 5456–5459.
37. Kováčik A, A. Vogel, J. Adler, P. Pullmannová, K. Vávrová, and D. Huster. 2018. Probing the role of ceramide hydroxylation in skin barrier lipid models by 2 H solid-state NMR spectroscopy and X-ray powder diffraction. *Biochim. Biophys. Acta Biomembranes.* **1860:**1162–1170.
38. Groen, D., G. S. Gooris, and J. A. Bouwstra. 2010. Model membranes prepared with ceramide EOS, cholesterol and free fatty acids form a unique lamellar phase. *Langmuir.* **26:** 4168–4175.
39. Wertz, P. W., D. C. Schwartzendruber, K. C. Madison, and D. T. Downing. 1987. Composition and morphology of epidermal cyst lipids. *J. Invest. Dermatol.* **89:** 419–425.
40. Školová, B., B. Janůšová, J. Zbytovská, G. Gooris, J. Bouwstra, P. Slepička, P. Berka, J. Roh, K. Palát, A. Hrabálek, and K. Vávrová. 2013. Ceramides in the skin lipid membranes: length matters. *Langmuir.* **29:** 15624–15633.
41. Pullmannová P, K. Staňková, M. Pospíšilová, B. Školová, J. Zbytovská, and K. Vávrová. 2014. Effects of sphingomyelin/ceramide ratio on the permeability and microstructure of model stratum corneum lipid membranes. *Biochim. Biophys. Acta Biomembranes.* **1838:** 2115–2126.
42. Pullmannová, P., L. Pavlíková, A. Kováčik, M. Sochorová, B. Školová, P. Slepička, J. Maixner, J. Zbytovská, and K. Vávrová. 2017. Permeability and microstructure of model stratum corneum lipid membranes containing ceramides with long (C16) and very long (C24) acyl chains. *Biophys. Chem.* **224:** 20–31.
43. Novotný, J., B. Janůšová, M. Novotný, A. Hrabálek, and K. Vávrová. 2009. Short-chain ceramides decrease skin barrier properties. *Skin Pharmacol. Physiol.* **22:** 22–30.
44. Craven, B. 1979. Pseudosymmetry in cholesterol monohydrate. *Acta Crystallogr. B.* **35:** 1123–1128.
45. Mojumdar, E. H., G. S. Gooris, and J. Bouwstra. 2015. Phase behavior of skin lipid mixtures: the effect of cholesterol on lipid organization. *Soft Matter.* **11:** 4326–4336.
46. Pullmannová, P., E. Ermakova, A. Kovacik, L. Opalka, J. Maixner, J. Zbytovska, N. Kučerka, and K. Vávrová. 2019. Long and very long lamellar phases in model stratum corneum lipid membranes. *J. Lipid Res.* **60:** 963–971.
47. White, S. H., D. Mirejovsky, and G. I. King. 1988. Structure of lamellar lipid domains and corneocyte envelopes of murine stratum-corneum - an X-ray-diffraction study. *Biochemistry.* **27:** 3725–3732.
48. Bouwstra, J., G. Gooris, W. Bras, and D. Downing. 1995. Lipid organization in pig stratum corneum. *J. Lipid Res.* **36:** 685–695.
49. Bouwstra, J., F. Dubbelaar, G. Gooris, and M. Ponec. 2000. The lipid organisation in the skin barrier. *Acta Derm. Venereol.* **208:** 23–30.
50. Boncheva M, F. Damien, and V. Normand. 2008. Molecular organization of the lipid matrix in intact Stratum corneum using ATR-FTIR spectroscopy. *Biochim. Biophys. Acta Biomembranes.* **1778:** 1344–1355.
51. Van Duzee, B. F. 1975. Thermal analysis of human stratum corneum. *J. Invest. Dermatol.* **65:** 404–408.
52. Golden, G. M., D. B. Guzek, R. R. Harris, J. E. McKie, and R. O. Potts. 1986. Lipid thermotropic transitions in human stratum corneum. *J. Invest. Dermatol.* **86:** 255–259.
53. Gay, C. L., R. H. Guy, G. M. Golden, V. H. Mak, and M. L. Francoeur. 1994. Characterization of low-temperature (ie,< 65 C) lipid transitions in human stratum corneum. *J. Invest. Dermatol.* **103:** 233–239.
54. Ongpipattanakul, B., M. L. Francoeur, and R. O. Potts. 1994. Polymorphism in stratum corneum lipids. *BBA-Biomembranes.* **1190:** 115–122.
55. Bouwstra, J. A., A. de Graaff, G. S. Gooris, J. Nijsse, J. W. Wiechers, and A. C. van Aelst. 2003. Water distribution and related morphology in human stratum corneum at different hydration levels. *J. Invest. Dermatol.* **120:** 750–758.
56. Bouwstra, J., G. Gooris, M. Salomons-de Vries, J. Van der Spek, and W. Bras. 1992. Structure of human stratum corneum as a function of temperature and hydration: a wide-angle X-ray diffraction study. *Int. J. Pharm.* **84:** 205–216.
57. Bouwstra J., G. Gooris, J. Brussee, M. A. Salomons-de Vries, and W. Bras. 1992. The influence of alkyl-azones on the ordering of the lamellae in human stratum corneum. *Int. J. Pharm.* **79:** 141–148.
58. Sochorová, M., K. Staňková, P. Pullmannová, A. Kováčik, J. Zbytovská, and K. Vávrová. 2017. Permeability barrier and microstructure of skin lipid membrane models of impaired glucosylceramide processing. *Sci. Rep.* **7:** 6470.
59. Crumrine, D., D. Khnykin, P. Krieg, M-Q. Man, A. Celli, T. M. Mauro, J. S. Wakefield, G. Menon, E. Mauldin, J. H. Miner, et al. 2019. Mutations in recessive congenital ichthyoses illuminate the origin and functions of the corneocyte lipid envelope. *J. Invest. Dermatol.* **139:** 760–768.
60. Angelova-Fischer, I., A. C. Mannheimer, A. Hinder, A. Ruether, A. Franke, R. H. Neubert, T. W. Fischer, and D. Zillikens. 2011. Distinct barrier integrity phenotypes in filaggrin-related atopic eczema following sequential tape stripping and lipid profiling. *Exp. Dermatol.* **20:** 351–356.
61. Matsumoto, M., H. Sugiura, and M. Uehara. 2000. Skin barrier function in patients with completely healed atopic dermatitis. *J. Dermatol. Sci.* **23:** 178–182.

62. Yoshiike, T., Y. Aikawa, J. Sindhvananda, H. Suto, K. Nishimura, T. Kawamoto, et al. 1993. Skin barrier defect in atopic dermatitis: increased permeability of the stratum corneum using dimethyl sulfoxide and theophylline. *J. Dermatol. Sci.* **5:** 92–96.
63. Halling-Overgaard, A. S., S. Kezic, I. Jakasa, K. Engebretsen, H. Maibach, and J. Thyssen. 2017. Skin absorption through atopic dermatitis skin: a systematic review. *Br. J. Dermatol.* **177:** 84–106.
64. van Smeden, J., M. Janssens, E. C. J. Kaye, P. J. Caspers, A. P. Lavrijsen, R. J. Vreeken, et al. 2014. The importance of free fatty acid chain length for the skin barrier function in atopic eczema patients. *Exp. Dermatol.* **23:** 45–52.
65. Kovacik, A., P. Pullmannová, J. Maixner, and K. Vavrova. 2018. Effects of ceramide and dihydroceramide stereochemistry at C-3 on the phase behavior and permeability of skin lipid membranes. *Langmuir.* **34:** 521–529.
66. Kessner, D., M. Kiselev, S. Dante, T. Hauß, P. Lersch, S. Wartewig, and R. H. Neubert. 2008. Arrangement of ceramide [EOS] in a stratum corneum lipid model matrix: new aspects revealed by neutron diffraction studies. *Eur. Biophys. J.* **37:** 989–999.
67. Mitragotri, S. 2003. Modeling skin permeability to hydrophilic and hydrophobic solutes based on four permeation pathways. *J. Control. Release.* **86:** 69–92.
68. Kiselev, M., E. Ermakova, A. Y. Gruzinov, and A. Zabelin. 2014. Formation of the long-periodicity phase in model membranes of the outermost layer of skin (Stratum corneum). *Crystallogr. Rep.* **59:** 112–116.
69. Schröter, A., D. Kessner, M. A. Kiselev, T. Hauß, S. Dante, and R. H. Neubert. 2009. Basic nanostructure of stratum corneum lipid matrices based on ceramides [EOS] and [AP]: a neutron diffraction study. *Biophys. J.* **97:** 1104–1114.
70. Rerek, M. E., H-C. Chen, B. Markovic, D. Van Wyck, P. Garidel, R. Mendelsohn, and D. J. Moore. 2001. Phytosphingosine and sphingosine ceramide headgroup hydrogen bonding: structural insights through thermotropic hydrogen/deuterium exchange. *J. Phys. Chem. B.* **105:** 9355–9362.
71. Rerek, M. E., D. Van Wyck, R. Mendelsohn, and D. J. Moore. 2005. FTIR spectroscopic studies of lipid dynamics in phytosphingosine ceramide models of the stratum corneum lipid matrix. *Chem. Phys. Lipids.* **134:** 51–58.